ELSEVIER

Polymer 41 (2000) 795–808

polymer

Compression and tension fatigue resistance of medical grade ultra high molecular weight polyethylene: the effect of morphology, sterilization, aging and temperature

D.A. Baker[a], R.S. Hastings[b], L. Pruitt[a,c,*]

[a]*Department of Mechanical Engineering, University of California, Berkeley, CA 94720, USA*
[b]*Research Division, DePuy Orthopaedics Inc., Warsaw, IN 46581, USA*
[c]*Department of Bioengineering, University of California, Berkeley, CA 94720, USA*

Received 10 September 1998; received in revised form 10 March 1999; accepted 14 March 1999

Abstract

It is shown in this study that polymer morphology, sterilization with or without accelerated aging, and temperature affect the fatigue crack propagation behavior of ultra high molecular weight polyethylene (UHMWPE). Changes in UHMWPE orthopedic implants due to sterilization and shelf aging are of great clinical interest and importance. In recent years, accelerated aging has been used to simulate shelf aging and post-sterilization oxidation in UHMWPE orthopedic components. In order to understand the role of sterilization and post-sterilization aging, two commercially available polymers (GUR4150HP and Hylamer®-M) with distinct morphologies were subjected to one of four sterilization techniques (gamma radiation in air, gamma radiation in vacuum, ethylene oxide gas, and gas plasma). Non-sterile samples were used as controls for all studies. Half the groups were tested in the unaged condition. The remaining samples were aged under accelerated conditions via elevated temperature (70°C) and oxygen pressure (5 atm) for 14 days to simulate five years of shelf aging. Subsequent to sterilization and aging treatments, specimens were subjected to cyclic compression loading followed by cyclic tensile loading in order to characterize the fatigue resistance. Scanning electron microscopy was used to provide an understanding of fatigue fracture mechanisms. Fourier transform infrared spectroscopy and density gradient column methods were used to determine the structural changes brought about by sterilization and aging. It is found in this work that accelerated aging causes a decrease in fatigue resistance regardless of sterilization method. Fatigue degradation is most severe for gamma radiation in air coupled with accelerated aging conditions. The results of this study have important implications for the design of fatigue resistant polymers used in medical applications.

Keywords: Ultra high molecular weight polyethylene; Fatigue; Morphology

1. Introduction

Although ultra high molecular weight polyethylene (UHMWPE) remains the material of choice for the bearing surface in total joint replacements it also limits the life of these components due to the generation of mechanically induced polymer debris. Contact between the UHMWPE and metallic components in a total joint arthroplasty results in complex stress distributions on the surface and within the polymer. It has been shown in a previous work that the maximum principal stress at a point near the surface of a total condylar type tibial knee component can range from 10 MPa of tension to 30 MPa of compression as the contact area sweeps across the surface during flexion [1]. Further, fully compressive cyclic loads have been shown to cause the inception and growth of mode I fatigue cracks in UHMWPE containing stress concentrations [2]. These compression fatigue cracks are the result of residual tensile stresses sustained at the notch as the polymer is unloaded from far-field compression [3,4]. Cracks that have initiated under cyclic compressive loading are then capable of propagating to critical lengths under the action of subsequent tensile stresses. Given the complex nature of cyclic loading in total knee replacements, fatigue damage sustained in normal gait action can lead to the inception and growth of subsurface cracks resulting in pitting and delamination of the UHMWPE components [5]. Understanding the variables affecting the compression and tension fatigue fracture resistance of UHMWPE will assist in the design of polymeric orthopedic devices offering long term structural integrity in vivo.

There are many pre-surgical factors that affect the fatigue resistance of the polymer and dictate the longevity of the

* Corresponding author. Tel.: +1-510-642-2595; fax: +1-510-643-5599.
E-mail address: lpruitt@newton.berkeley.edu (L. Pruitt)

0032-3861/00/$ - see front matter
PII: S0032-3861(99)00199-8

implant. These variables include the resin type and processing conditions, the method of sterilization, and post-sterilization aging prior to implantation. The starting resin and processing conditions play a critical role in the fatigue resistance of the orthopedic component by dictating the initial polymer properties including molecular weight, crystallinity, density and morphology. These molecular variables are known to have a profound affect on the fatigue performance [6,7]. Further, the processing conditions associated with the ram extrusion or compression molding of the resin can alter the polymer morphology, or degree of lamellae stacking or texture, which can result in substantial differences in fatigue behavior [7].

Once the orthopedic components have been manufactured, the device must be sterilized prior to implantation. There are three basic classes of sterilization: high temperature, gases, and ionizing radiation. High temperature sterilization includes steam or autoclaving but is unacceptable for UHMWPE due to the low melting point of the polymer. Common methods of non-ionizing sterilization methods include ethylene oxide gas and gas plasma. Ethylene oxide [8] and gas plasma [9] sterilization are known to cause little or no degradation to the mechanical properties of the UHMWPE. Gamma radiation, typically a minimum of 25 kGy from a ^{60}Co source, is a common sterilization method used widely by the medical industry. This ionizing sterilization method can be done in air or in an inert environment. Numerous researchers [10–12] have shown gamma radiation in air to be the main reason in degrading the mechanical and structural integrity of UHMWPE. Conversely, others have shown that gamma radiation in an inert environment can be beneficial to the wear properties of the polymer [13–16]. This apparent dichotomy is due to the relative dominance of various reaction schemes and kinetics of free radicals generated through ionizing radiation [17]. While scission and crosslinking always occur to some degree in UHMWPE subjected to gamma radiation, the presence of oxygen during radiation and available in the surrounding environment after sterilization results in chain scission mechanisms and oxidative degradation. In the absence of oxygen during ionizing radiation, crosslinking mechanisms are favored although some degree of scission and oxidation still occurs. If one can control the ionization process and reaction kinetics to favor crosslinking then one can develop a more stable polymer that resists oxidation and time dependent degradation. Further, crosslinking has shown great promise in reducing the wear of UHMWPE [14,15] and this has prompted many to believe that gamma radiation in an inert environment is an acceptable sterilization method for orthopedics. While crosslinking has shown great promise in improving tribological properties [16], it has remained unclear whether the same benefit will be realized in the fatigue resistance of UHMWPE. Recent studies [18,19], however, indicate that gamma radiation in an inert environment may not offer any improvement to the fatigue resistance of UHMWPE but rather may result in severe embrittlement of the polymer. This is an important finding for UHMWPE components used in total knee replacements where fatigue loading has been shown to play a critical role on the longevity of the prosthesis [20].

Shelf aging particularly when the component has been sterilized by ionizing radiation [17] is another factor that affects the fatigue properties and implant life. A recent tool developed to aid in the evaluation of post-sterilization shelf aging is accelerated, or artificial aging [21–23]. The motive behind artificial aging is to obtain predictions of long term performance within a shortened test period. Some current accelerated aging protocols involve an elevated temperature coupled with either a heating rate [21] or an elevated oxygen pressure [22]. It has been stated that for artificial aging to be valid the material state attained via accelerated aging and the mechanisms behind the physical changes must be the same as when naturally aged [23–25]. Care has been taken to show that artificially aged UHMWPE specimens have similar densities, oxidation indices, subsurface oxidation profiles, and monotonic mechanical properties; however, few tests have been done to examine the correlation of such structural changes with the fatigue behavior of the polymer. Specifically, it is of interest to know how accelerated aging affects the ability of the polymer to resist crack growth when subjected to both cyclic compression and tension loading.

Testing conditions are also expected to affect the fatigue behavior of UHMWPE. While the majority of fatigue crack propagation resistance research has been performed at room temperature under sinusoidal loading conditions, it is well known that polymer fatigue resistance is highly sensitive to load ratio, waveform, and frequency [18,26]. Further, the majority of fatigue characterization has been performed in laboratory air conditions despite the fact that UHMWPE is a low melting point viscoplastic polymer whose mechanical properties are likely to be affected by temperature. This is of clinical concern as orthopedic components are cyclically loaded in vivo at body temperature (37°C). To date little crack propagation data exists for UHMWPE tested under body temperature conditions [27].

The primary objectives of this study are to understand the role of polymer morphology, sterilization method, accelerated aging, and test temperatures on the fatigue fracture resistance of medical grade UHMWPE. The two polymers used for this study are GUR4150HP and Hylamer®-M. The choice of these two polymers stems from their differences in morphology, crystallinity, and density brought about through distinct processing conditions (pressure and temperature) of nominally identical starting resins. Four sterilization protocols are considered in this study: gamma radiation in air, gamma radiation in an inert environment, ethylene oxide gas, and gas plasma. Non-sterile materials are used as a control for both polymers. The aim of this work is to determine which polymer morphologies and sterilization methods offer the best resistance to fatigue crack propagation for long term structural integrity in total

Table 1
Physical properties of GUR4150HP and Hylamer®-M

Property	GUR4150HP	Hylamer®-M
Molecular weight	3–6 million g/mol	3–6 million g/mol
Crystallinity	45–50%	55–60%
Density	0.93–0.935	0.94–0.946
Ultimate tensile strength (21°C)	42–44 MPa	38–40 MPa
Ultimate tensile strength (37°C)	36 MPa	41 MPa
Yield strength (21°C)	20–23 MPa	27–30 MPa
Yield strength (37°C)	21 MPa	25 MPa
Elastic modulus (21°C)	1.0–1.39 GPa	2.0–2.5 GPa
Elastic modulus (37°C)	0.67 GPa	1.1–1.2 GPa
Elongation at break (21°C)	330%	370%
Elongation at break (37°C)	375%	405%
Shore D hardness (21°C)	60–65	64–69

joint replacements. It is also shown in this paper that the accelerated aging process affects the fatigue crack propagation behavior.

2. Experimental methods

2.1. Materials

The materials used in this study were ram extruded GUR4150HP (GUR) and Hylamer®-M medical grade UHMWPE. The Hylamer®-M used was GUR4150HP that had been post-processed under high temperature and pressure to increase the size and amount of crystalline regions leading to different properties. The room and body temperature properties are summarized in Table 1 for both polymers. All materials were supplied by DePuy-DuPont (Warsaw, Indiana). The extruded UHMWPE was machined into compact tension specimens prior to sterilization. Twenty compact tension specimens were prepared for each material group. Five groups were studied for the GUR: non-sterile, 25 kGy of gamma radiation in an air environment (gamma-air), 25 kGy of gamma radiation in a vacuum environment after flushing with nitrogen gas (gamma-inert), gas plasma, and ethylene oxide gas. For the Hylamer®-M, four groups were studied: non-sterile, gamma-air, gamma-inert, and gas plasma. Ethylene oxide gas was examined for the unaged Hylamer®-M for comparative purposes only (ethylene oxide treatment is not a clinically relevant sterilization condition for Hylamer®-M). After sterilization, half of each group (10 specimens) was subjected to 14 days of accelerated aging at 70°C and 5 atm O_2. The second half of each group remained unaged. The unaged gamma-inert specimens were individually vacuum-sealed in order to minimize oxidation. A total of 18 groups were investigated for this study.

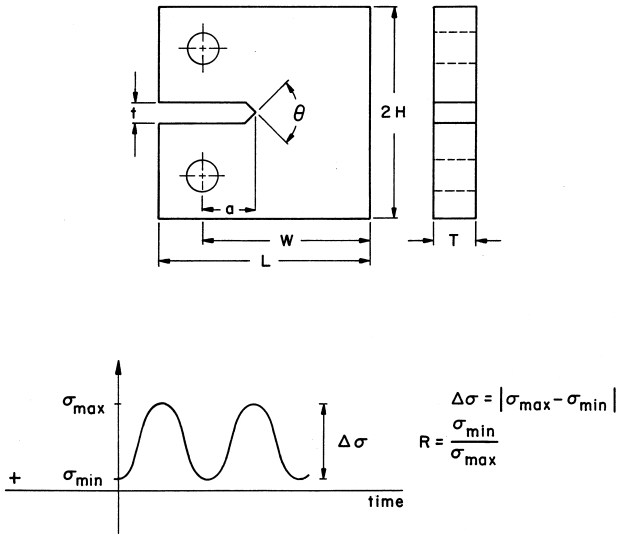

Fig. 1. Schematic illustration of the compact tension specimen used in the fatigue studies.

All fatigue tests were performed on compact tension specimens with the following geometry [7]: width, $W = 25.4$ mm; length, $L = 31.75$ mm; height, $2H = 31.75$ mm; initial notch length, $a = 8.89$ mm; notch width, $t = 3.12$ mm; included notch angle, $\theta = 60°$; notch root radius, $\rho = 0.127$ mm; hole diameter, $d = 5.334$ mm; distance between holes = 18.52 mm; and thickness, $T = 8.13$ mm. A schematic of this specimen geometry is provided in Fig. 1. All specimens were machined such that the crack growth would be perpendicular to the extrusion direction. Fatigue tests were performed in a recirculating deionized 37°C water bath (made of Lexan) on a servohydraulic Instron 8511 using a sinusoidal wave function at a frequency of 5 Hz. In order to evaluate the effect of test temperature, the non-sterile GUR specimens were characterized in 37(±1)°C water, near-room temperature water 24(±1)°C, and room temperature air 22(±1)°C. Fatigue resistance was characterized for both cyclic compression and cyclic tension loading conditions. The stress ratio or R-ratio (R is defined as the minimum stress to the maximum stress of the fatigue cycle and is schematically illustrated in Fig. 1) used in this study was $R = 30$ for compression fatigue and $R = 0.1$ for tension fatigue.

2.2. Compression fatigue

The fatigue tests were performed using compression platens to apply the far-field load perpendicular to the plane of the notch. The fully compressive fatigue tests were performed using a load ratio of $R = 30$ (−0.22 to −6.5 MPa). Crack growth was monitored using an Olympus BH-2 microscope. Compression fatigue tests were terminated upon saturation of the fatigue crack, dictated by the zone of residual tension ahead of the notch tip [4]. Saturated lengths were noted for all material groups.

2.3. Tension fatigue

Fully tensile fatigue tests were conducted on the compact tension specimens with existing pre-crack lengths dictated by the saturation lengths resulting from cyclic compression.

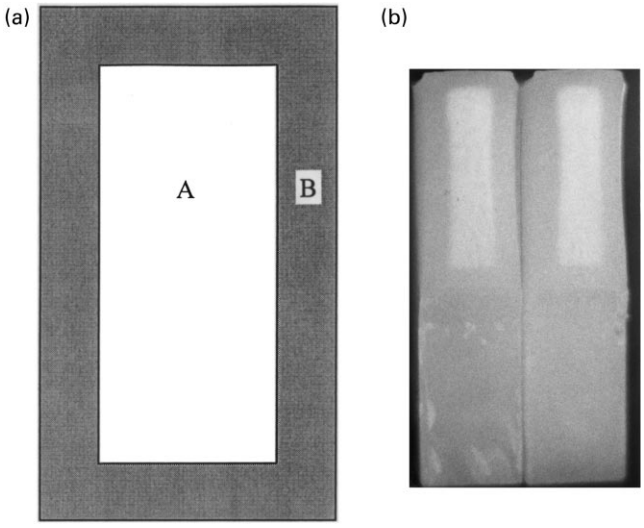

Fig. 2. (a) Schematic illustration of the transition of optical translucence in the aged polymers. Interior density was taken in region A, exterior density was taken in region B; (b) Optical micrograph depicting the transition observed on the fracture surface of Hylamer®-M sterilized by gas plasma and subjected to accelerated aging.

Tests were performed using standard pin loading using a load ratio of $R = 0.1$. Careful attention was paid to locate the inception of crack propagation and was defined as stress intensity ranges corresponding to a crack growth rate of 10^{-6} mm/cycle (ΔK_{incept}). Tension fatigue tests were performed under constant stress amplitude conditions throughout the Paris regime (where $da/dN = C(\Delta K)^m$ holds). The slopes (m) were calculated for each data set using a best-fit straight line through all data between 10^{-6} and 3×10^{-4} mm/cycle.

2.4. Fractography

In order to provide a micromechanistic link to the fatigue fracture resistance, fractography was performed at the completion of tension fatigue testing. Fractured specimens from each of the 18 groups were sputter-coated with Au–Pd and examined using a JEOL 35CF scanning electron microscope (SEM). Attention was paid to different fracture mechanisms observed amongst the groups. Additional microscopy was performed using a JOEL 6301 field emission microscope (FEM) to characterize the morphology. For FEM, specimens were prepared using a standard permanganate etch to preferentially remove the amorphous regions of the polymer. All polymer surfaces were then coated with gold prior to imaging.

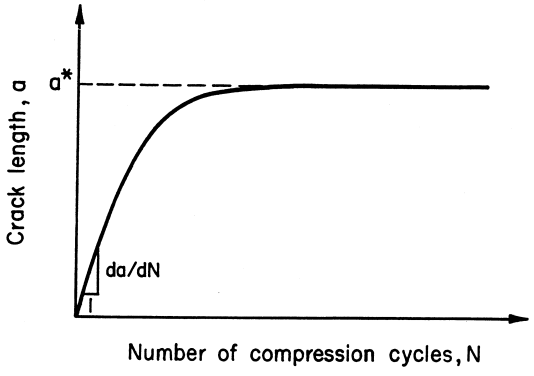

Fig. 3. Schematic of the compression fatigue crack growth behavior of GUR4150HP and Hylamer®-M.

2.5. Density gradient column measurements

Following fatigue testing, fractured specimens were sectioned for density characterization using a density gradient column (DGC) of distilled water and isopropanol. The column was prepared according to ASTM D1505-85 standard. Two samples, each approximately $2 \times 2 \times 2$ mm^3, were studied for each unaged material group and four to six samples were studied for each aged material group. All samples from the aged specimens were taken from either region A or B as shown in Fig. 2.

2.6. Fourier transform infrared spectroscopy

Fourier transform infrared spectroscopy (FTIR) was performed on a BIO-RAD UMA 250 at DePuy Orthopaedics Inc. (Warsaw, IN). Three 200 μm samples were sectioned from a representative fractured compact tension specimen in each of the aged material groups in order to determine the oxidation index of the aged specimens. These slices were oriented under the FTIR microscope so that a depth profile could be performed. Measurements were taken at 50 μm intervals to a depth of 200 μm and then at intervals of 100 μm up to a maximum depth of 4000 μm. Carbonyl area/mil was calculated using the absorbance spectrum between the 1800 and 1660 cm^{-1} wavenumbers. Baseline minima for the area calculation were found between the 1680–1630 and 1800–1750 cm^{-1} wavenumbers. The data were normalized for thickness (1 mil) using the peak height of the 4250 cm^{-1} wavenumber measured from the line established by the 4297 cm^{-1} wavenumber. Ketone absorbance/mil was calculated using the same baseline minima as the carbonyl area and then looking for the maximum absorbance between the 1720 and 1710 cm^{-1} wavenumbers. This value was also normalized using the 4250 cm^{-1} peak height.

3. Results

3.1. Compression fatigue

All compression fatigue cracks initiate in the plane of the notch and grow perpendicular to the compression axis. For all specimens, the compression fatigue cracks propagate at a progressively diminishing rate before arresting at a crack saturation length, a^*. Fig. 3 schematically depicts the compression fatigue crack length as a function of number of loading cycles. The average saturation lengths, a^*,

Table 2
Summary of compression and tension fatigue properties: (a) compression and tension fatigue properties for GUR4150HP; (b) compression and tension fatigue for Hylamer®-M; and (c) the effect of temperature (non-sterile GUR4150HP)

	Compression fatigue, saturation length a^* (mm)	Tension fatigue	
		ΔK_{incept} (MPa$\sqrt{m}$)[a]	Slope, m[b]
(a) GUR4150HP			
Non-sterile (unaged)	0.11	2.01	21.4
Non-sterile (aged)	0.08	1.80	19.3
Plasma (unaged)	0.07	2.01	23.4
Plasma (aged)	0.08	1.81	17.1
EtO (unaged)	0.09	1.90	19.3
EtO (aged)	0.08	1.71	14.9
Gamma-air (unaged)	0.08	1.51	24.3
Gamma-air (aged)	0.04	0.90	[c]
Gamma-inert (unaged)	0.07	1.51	23.1
Gamma-inert (aged)	0.04	1.50	46.4
(b) Hylamer®-M			
Non-sterile (unaged)	0.05	2.51	30.9
Non-sterile (aged)	0.05	2.44	33.6
Plasma (unaged)	0.04	2.49	21.4
Plasma (aged)	0.04	2.39	27.0[d]
EtO (unaged)	0.04	2.40	27.9
EtO (aged)	–	–	–
Gamma-air (unaged)	0.03	2.21	38.9
Gamma-air (aged)	0.03	1.00	[c]
Gamma-inert (unaged)	0.03	2.16	48.1
Gamma-inert (aged)	0.03	1.61	295.0
(c) GUR4150HP			
Non-sterile (37°C, H_2O)	0.11	2.01	21.4
Non-sterile (25°C, H_2O)	0.06	2.17	19.2
Non-sterile (22°C, air)	0.05	2.20	22.4

[a] Defined at $da/dN \approx 10^{-6}$.
[b] Defined for $10^{-6} \leq da/dN \leq 3 \times 10^{-4}$.
[c] No slope calculated due to surface cracking and fracture instability.
[d] Defined for $10^{-6} \leq da/dN \leq 3 \times 10^{-3}$.

measured from the compression fatigue tests on the aged and unaged GUR4150HP (GUR) are given in Table 2(a). The unaged non-sterile group results in the largest saturation length for the GUR, $a^* = 0.11$ mm. All sterilization processes cause a decrease in saturation length from the non-sterile, unaged material group. Artificial aging also engenders a substantial decrease in a^* for the non-sterile and both gamma sterilized material groups. The most substantial decrease in a^* from the unaged non-sterile group is seen for the aged gamma-air and aged gamma-inert, $a^* = 0.04$ mm.

Table 2(b) gives the average saturation lengths for both unaged and aged Hylamer®-M. The unaged non-sterile group has the largest saturation length for the Hylamer®-M, $a^* = 0.05$ mm. Gamma sterilization results in the most notable decrease in saturation length, resulting in drop to $a^* = 0.03$ mm for both the gamma-air and gamma-inert specimens. Accelerated aging causes no change in saturation length within each material group.

Table 2(c) provides the average saturation lengths for the non-sterile GUR as a function of temperature. The saturation length clearly decreases with decreasing temperature. The 37(±1)°C group has the largest saturation length, $a^* = 0.11$ mm. The 22(±1)°C group has the smallest saturation length with $a^* = 0.05$ mm.

3.2. Tension fatigue

Table 2(a) summarizes the stress intensity ranges necessary for crack inception (ΔK_{incept}) and the slopes of the growth rates for GUR. Fig. 4(a) shows the tensile fatigue crack propagation rate, da/dN, as a function of crack driving force, ΔK, for the unaged GUR. It is seen in this figure that non-sterile and gas plasma specimens are the most resistant to crack propagation followed by EtO sterilization. Gamma sterilization (air and inert) has the most pronounced effects on the initial ΔK in the unaged material groups. It is clear from this plot that radiation results in a drop in crack inception from 2.01 MPa$\sqrt{m}$ (for the non-sterile specimens) to 1.51 MPa$\sqrt{m}$ for both gamma-air and gamma-inert specimens. Fig. 4(b) shows da/dN as a function of ΔK for the accelerated aged GUR. Here, it is seen that artificial aging causes a further decrease in initial ΔK values for all material groups, however it is most severe in the gamma-air material

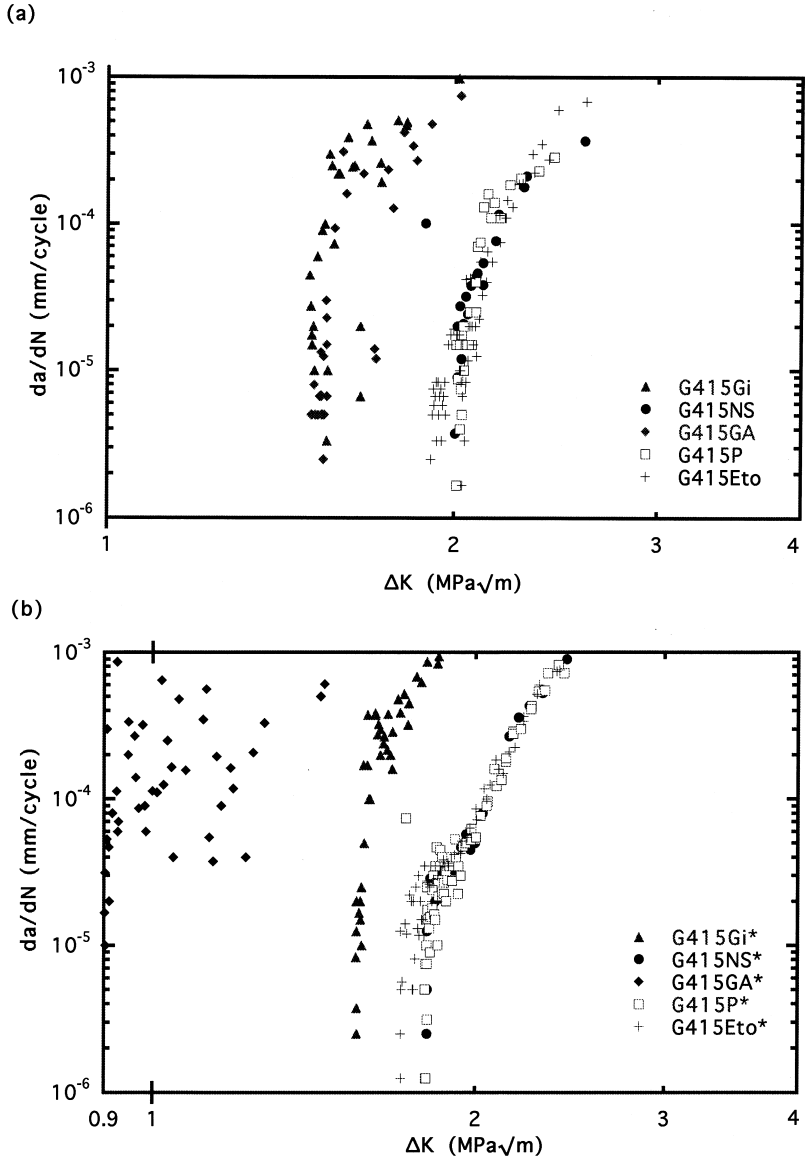

Fig. 4. Plots of tension crack propagation rates as a function of stress intensity range. The effect of sterilization is shown for the: (a) unaged GUR4150HP; (b) aged GUR4150HP; (c) unaged Hylamer®-M; and (d) aged Hylamer®-M. The effect of temperature is shown for (e) non-sterile GUR4150HP. (Note: NS = non-sterile, P = gas plasma sterilized, EtO = ethylene oxide sterilized, Ga = gamma sterilized in air, Gi = gamma sterilized in an inert environment, and * denotes accelerated aging.)

group where the initial ΔK decreases from 1.51 (unaged) to 0.90 MPa$\sqrt{m}$ (aged). Artificial aging also causes a decrease, albeit less drastic, in the non-sterile and gas plasma material groups reducing the necessary ΔK for crack inception from 2.01 to 1.80 MPa$\sqrt{m}$ for the non-sterile specimens and from 2.01 to 1.81 MPa$\sqrt{m}$ for the gas plasma sterilized specimens.

Table 2(b) summarizes the ΔK_{incept} values and the slopes of the fatigue plots for crack growth rates for Hylamer®-M. Fig. 4(c) shows the crack growth rate as a function of crack driving force for unaged Hylamer®-M. It is seen in this figure that non-sterile and gas plasma material groups are the most resistant to fatigue crack propagation and are followed closely by EtO sterilization. Again, gamma sterilization has the most pronounced effects on the initial ΔK in the unaged material groups. Gamma sterilization decreases ΔK for inception of crack propagation from 2.51 MPa$\sqrt{m}$ for the non-sterile specimens to 2.21 and 2.16 MPa$\sqrt{m}$ for the gamma-air and gamma-inert specimens, respectively. Fig. 4(d) shows the fatigue behavior for the accelerated aged Hylamer®-M. Once more, artificial aging brings about a decrease in initial ΔK values for all material groups, however it is seen that aging has the most pronounced effects on both gamma sterilized material groups. The most substantial reduction occurs in the gamma-air group resulting in a decrease from 2.21 to 1.00 MPa$\sqrt{m}$. Aging also gives rise to a slight decrease in the non-sterile and gas plasma material groups reducing the necessary ΔK for

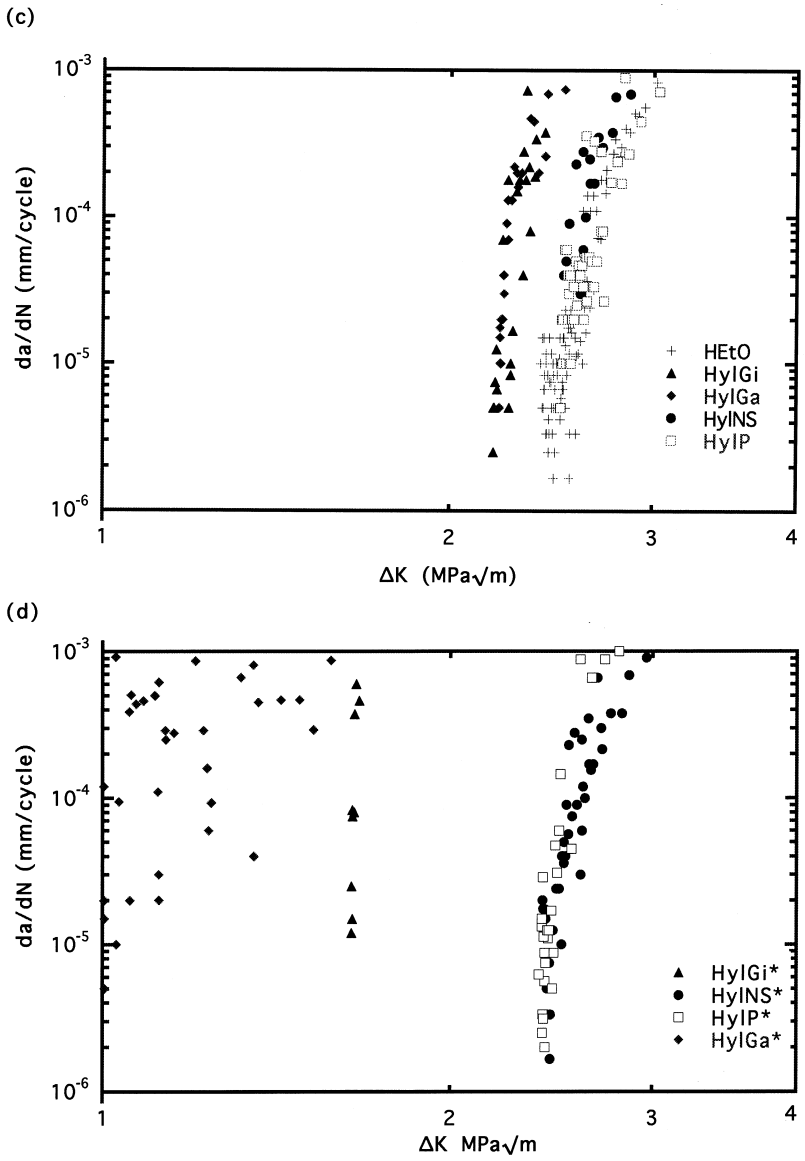

Fig. 4. (*continued*)

crack inception from 2.51 to 2.44 MPa$\sqrt{m}$ for the non-sterile case, and from 2.49 to 2.39 MPa$\sqrt{m}$ for the plasma sterilized specimens.

Table 2(c) summarizes the ΔK_{incept} values and the crack propagation slopes for GUR as a function of temperature. Fig. 4(e) shows the tensile fatigue crack propagation behavior of the non-sterile GUR for three temperature conditions: 37(±1)°C in water, 25(±1)°C in water, and 22(±1)°C in air. It is seen in this figure that the room temperature specimens are the most resistant to crack propagation while the body temperature condition results in a reduction of ΔK_{incept}.

3.3. Fractography of unaged specimens

Representative SEM micrographs for the unaged material groups are shown in Figs. 5 and 6. For all micrographs, crack propagation is from left to right. Fig. 5(a) shows an electron micrograph of the representative fracture mechanisms operating in the Paris regime for the gas plasma sterilized GUR specimens. This fractograph exhibits the well documented ductile criss-cross or diamond patterns observed in pristine UHMWPE [26]. These same criss-cross features associated with lamellae tearing are found in the non-sterile and ethylene oxide sterilized groups. Similar mechanisms are observed (albeit at a slightly smaller scale) for the unaged Hylamer®-M groups subjected to gas plasma (as seen in Fig. 5(b)), ethylene oxide, or no sterilization. Gamma radiation (air or inert) results in a visible reduction in the level of ductile features in both polymers. Fig. 6(a) and (b) shows the Paris regime fatigue micromechanisms for the gamma-air sterilized GUR and

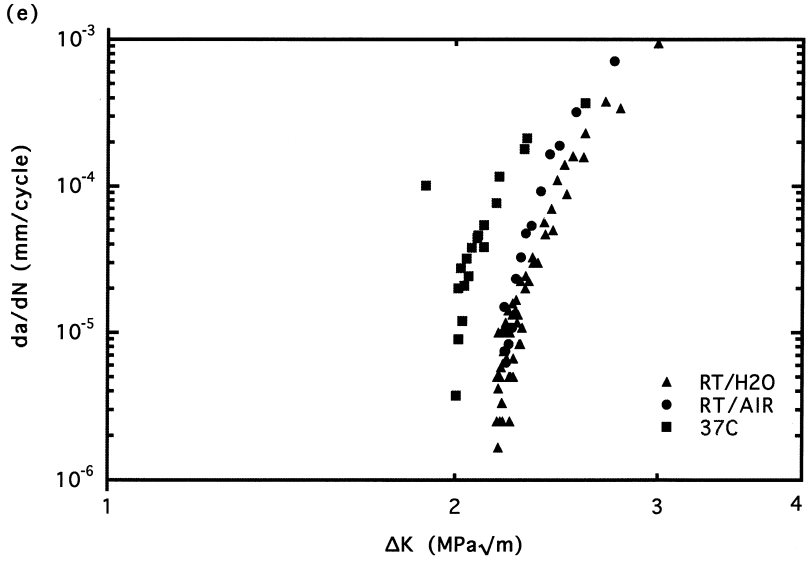

Fig. 4. (*continued*)

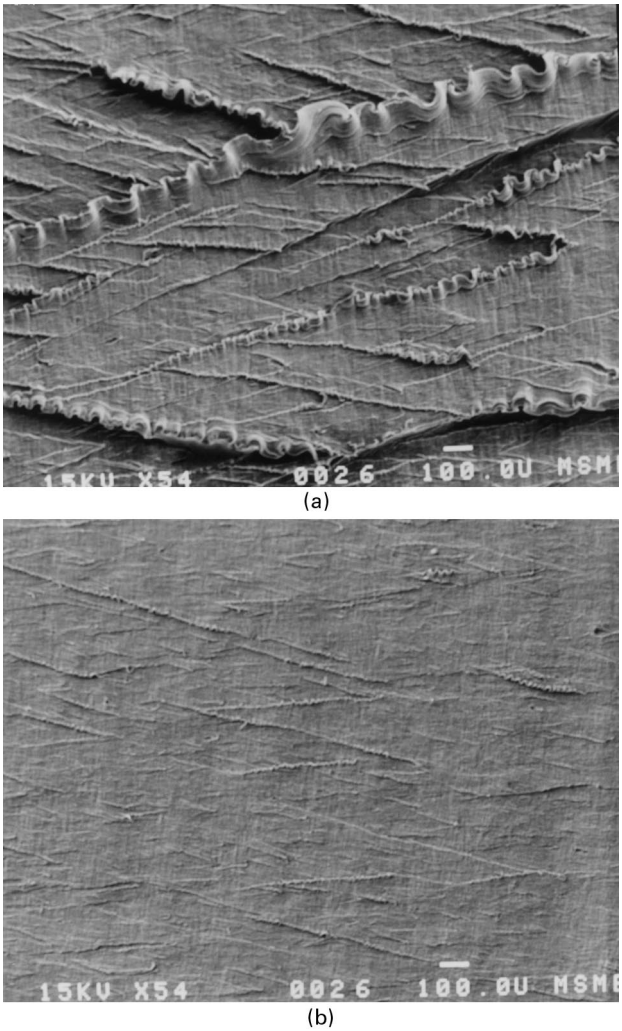

Fig. 5. Scanning electron micrograph of the fracture mechanisms in the Paris regime for gas plasma sterilized: (a) GUR4150HP; and (b) Hylamer®-M. The fatigue crack growth direction is left to right.

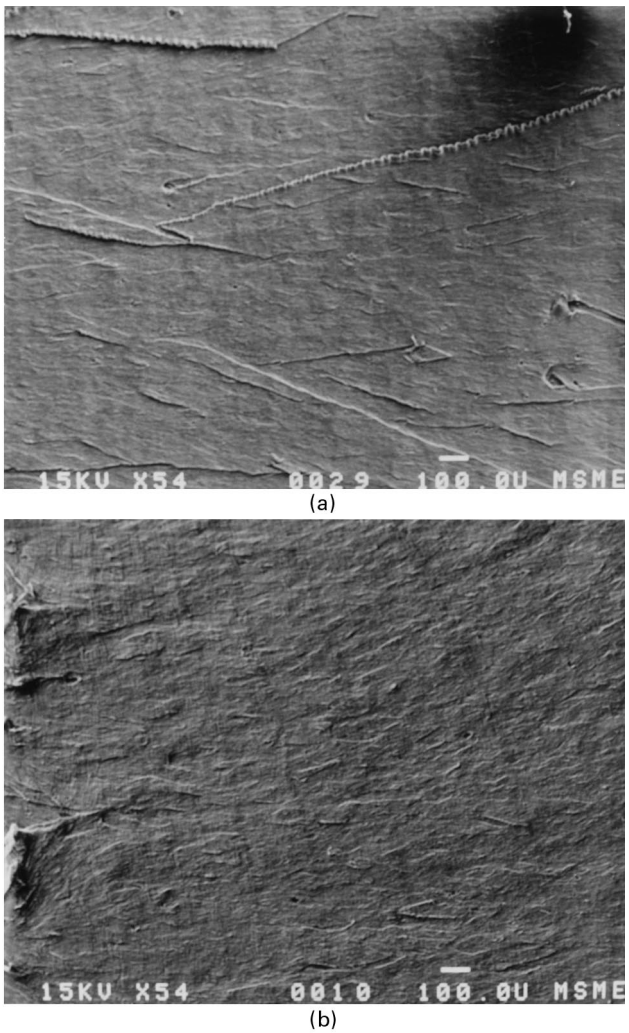

Fig. 6. Scanning electron micrograph of the fracture mechanisms in the Paris regime for the gamma-air sterilized: (a) GUR4150HP; and (b) Hylamer®-M. The fatigue crack growth direction is left to right.

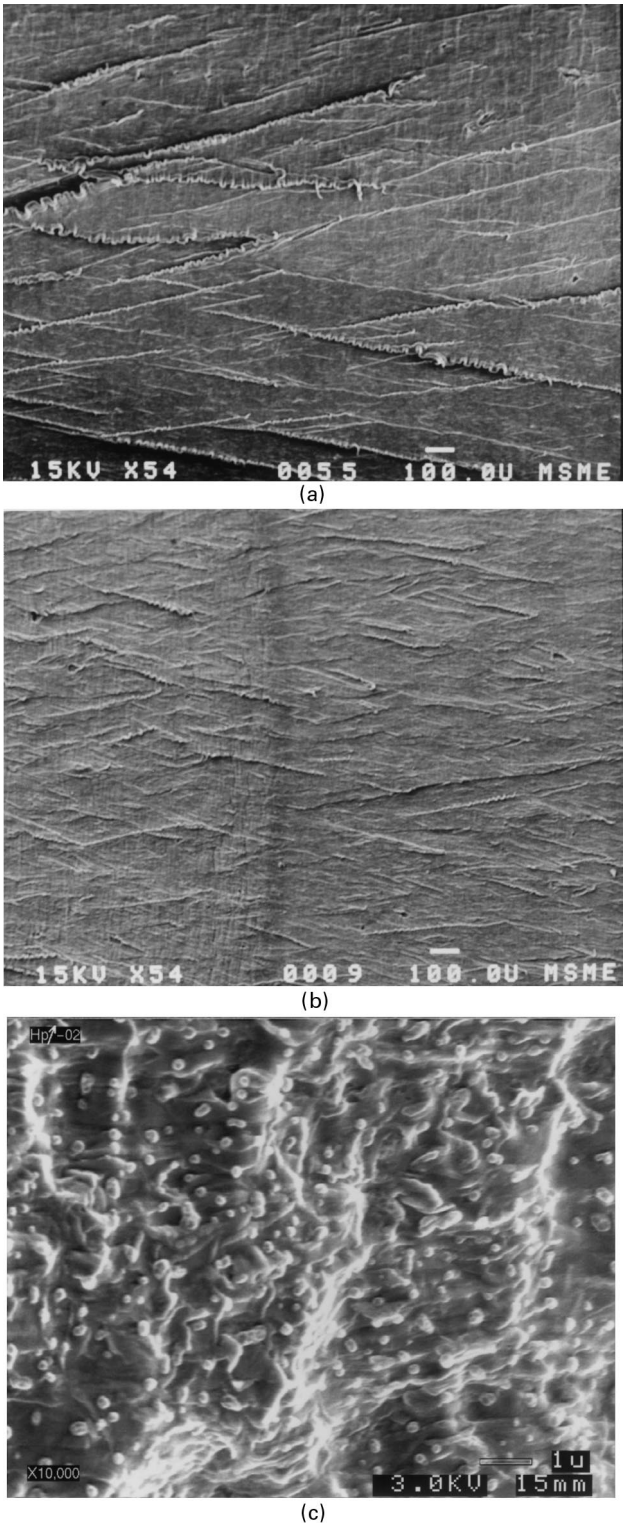

Fig. 7. Scanning electron micrograph of the fracture mechanisms in the Paris regime for the aged gas plasma sterilized (a) GUR4150HP; and Hylamer®-M at (b) low and (c) high magnification depicting the ductile tearing of polymer fibrils. The fatigue crack growth direction is left to right.

Hylamer®-M, respectively. Similar features are detected in the specimens that were gamma sterilized in an inert environment.

3.4. Fractography of aged specimens

Representative SEM micrographs for the aged material groups are shown in Figs. 7–10. For all micrographs, crack propagation is from left to right. It should be noted that all of the aged fracture surfaces exhibit to some degree a white inner region and a more translucent outer ring as shown in Fig. 1. Accelerated aging has little effect on the non-sterile, gas plasma, and ethylene oxide sterilized material groups but results in drastic alterations to the gamma sterilized groups. While these optical discolorations are not detectable in the SEM it is evident that different fracture mechanisms operate in the interior of the gamma radiated specimens. No such mechanistic distinctions are made for specimens not subjected to ionizing radiation. Figs. 7(a) and (b) demonstrate that the classic diamond-like features are preserved for materials not subjected to radiation. Fig. 7(a) depicts the Paris regime mechanisms for the aged plasma sterilized GUR specimens. Fig. 7(b) provides a low magnification image of the Paris regime mechanisms for the aged plasma sterilized Hylamer®-M specimens. Fig. 7(c) is a high magnification field emission fractograph of the gas plasma sterilized and accelerated aged Hylamer®-M depicting the ductile tearing of polymer fibrils. Unlike the non-ionized groups, substantial changes in micromechanisms associated with accelerated aging are noted in the gamma sterilized materials. Fig. 8(a) shows the entire fracture surface and the distinct micromechanisms from the near surface to the interior of the gamma-air sterilized GUR specimen. Higher magnification images of the scallops and cellular-like features associated with gamma radiation combined with accelerated aging of GUR specimens are shown in Fig. 8(b) and (c), respectively. Similar features are observed for the Hylamer®-M specimens subjected to gamma radiation in air and accelerated aging (as shown in Fig. 9(a) and (b)). Radiation in an inert atmosphere results in a reduced severity of the transition zone as seen in the full fracture surface of the GUR and Hylamer®-M specimens (Fig. 10(a)). However, the inert atmosphere does not diminish the propensity of scallop markings on the fracture surfaces (Fig. 10(b)).

3.5. Morphology

Fig. 11(a) and (b) are field emission micrographs depicting the lamellae structure of the GUR4150HP and Hylamer®-M, respectively. Note the larger crystalline structures in the Hylamer®-M associated with the higher temperature and pressure process. The larger crystalline lamellae correlate with the increased crystallinity, density, modulus, and yield strength of this polymer (Table 1).

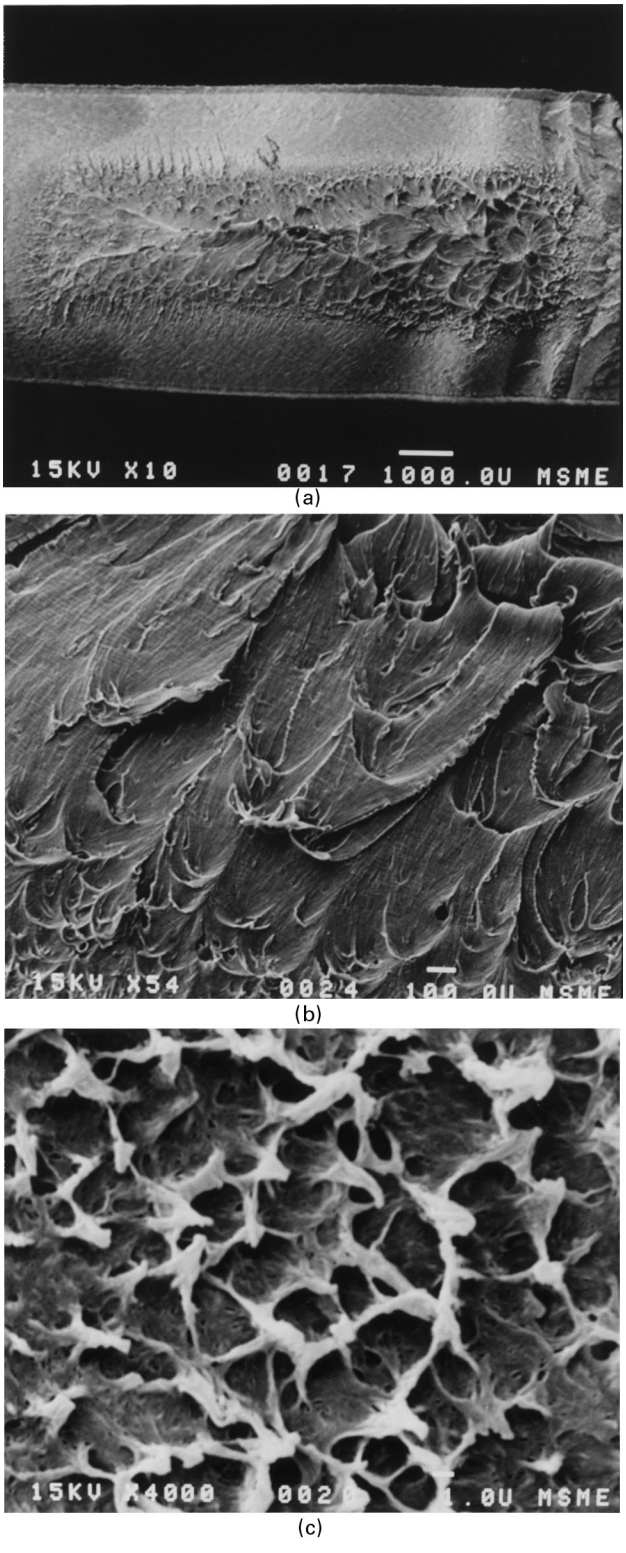

Fig. 8. Scanning electron micrograph of the (a) fracture surface for the aged gamma-air sterilized GUR4150HP. Note the change in micromechanism from the surface through the interior and the presence of (b) scallop markings and (c) cellular features with the remnants of numerous, small fibrils oriented orthogonal to the crack plane. The fatigue crack growth direction is left to right.

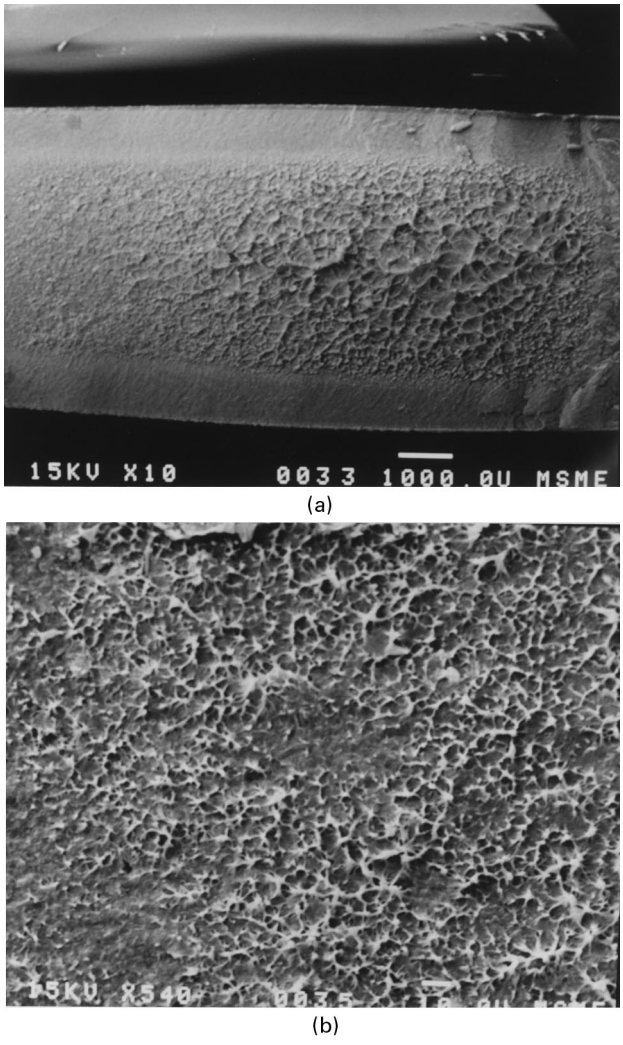

Fig. 9. Scanning electron micrograph of the (a) fracture surface for the aged gamma-air sterilized Hylamer®-M. Note the change in micromechanism from the surface through the interior and the presence of the (b) cellular structure. The fatigue crack growth direction is left to right.

3.6. Density gradient column measurements

Densities taken from representative fracture surfaces in each material group are summarized in Table 3. For the aged specimens, densities are measured for both the inner (region A) and outermost (region B) areas of the fracture plane as denoted in Fig. 2(a). The densities are determined for the cross section in an attempt to correlate the discoloration associated with accelerated aging (Fig. 2(a) and (b)) and the density of the polymer. Substantial differences in density are found between the inner and outer regions in both the GUR and Hylamer®-M when subjected to gamma radiation in air and subsequently aged. Fig. 12 clearly demonstrates a substantial increase in density in the outer region of the gamma radiated samples.

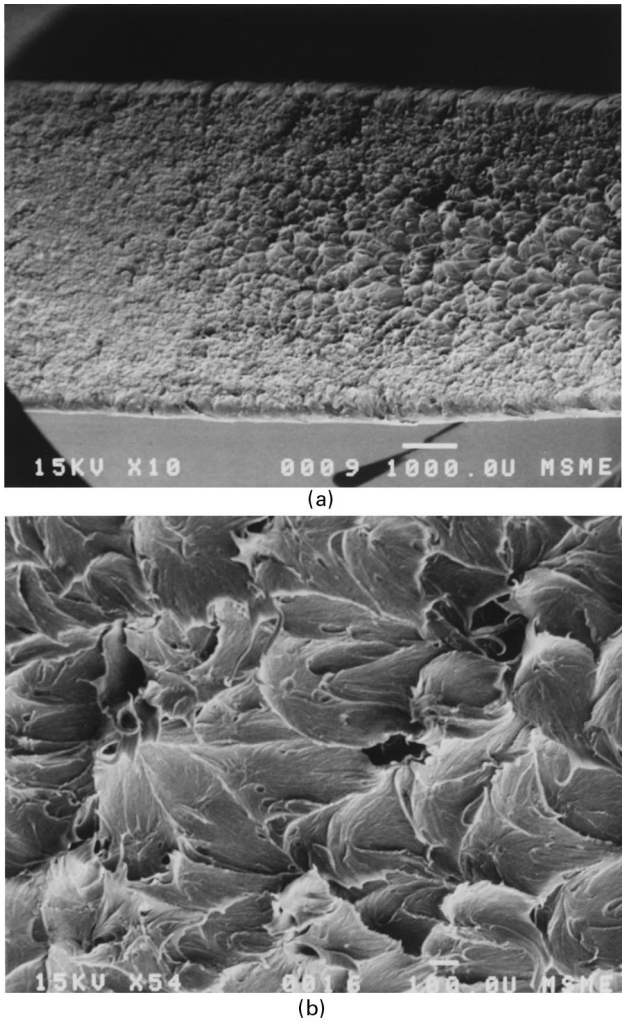

Fig. 10. Scanning electron micrograph of the (a) fracture surface for the aged gamma-inert sterilized Hylamer®-M. Note the presence of (b) scallop features. The fatigue crack growth direction is left to right.

3.7. Fourier transform infra-red spectroscopy

Table 4 summarizes the FTIR data for the aged material groups with unaged non-sterile used as the control. It can be seen through examination of the peak carbonyl area/mil that the Hylamer®-M exhibits the least amount of oxidation when compared to the GUR material group counterpart. Similar trends are noted for the ketone absorbance/mil. This is expected due to the larger crystalline lamellae of the Hylamer®-M. For both the GUR and Hylamer®-M, the non-sterile and non-ionizing sterilization methods result in very little oxidation after accelerated aging. This is in contrast to the ionizing sterilization methods that show an increased level of oxidation after aging. Specifically, the gamma-air sterilization and subsequent aging lead to severe oxidation. Both the GUR and Hylamer®-M aged gamma-air and gamma-inert specimens exhibit subsurface oxidation peaks.

4. Discussion

For all material groups, the compression fatigue cracks advance at a decelerating rate until reaching a characteristic saturation length, a^*. The driving force for crack inception under cyclic compressive loading is the generation of residual tensile stresses ahead of the notch [4]. As the crack progresses it eventually saturates due to the combination of crack closure and the imposing far-field compressive loads. Once the residual tensile field is exhausted, the crack has insufficient driving force for crack advance. The magnitude of the saturation crack length is dictated by near-tip stresses and levels of retained permanent or plastic strain upon unloading from far-field compression. The saturation length is strongly affected by local micromechanisms and levels of damage sustained at the notch tip. Thus it is expected that different yield behavior between the two polymers and for different temperatures will affect the saturation lengths. It is apparent from Table 2 that for identical loading conditions Hylamer®-M exhibits substantially less crack growth than the GUR4150HP. Further, the lower temperature tests result in smaller saturation lengths. This behavior is the result of the increased yield stress associated with the modified structure (resulting in enhanced lamellae thickness, crystallinity, and density) for the Hylamer®-M (Table 1) or associated with a decreased temperature. The higher yield strengths result in a reduction of plastic strain at the notch tip. The reduction in retained permanent deformation results in a decrease in the residual tensile stresses upon unloading from far-field compression. It is expected that any treatment which reduces the near-tip strains for the same notch geometry and near-tip stresses will decrease the level of crack growth under fully compressive fatigue conditions. This trend is seen in the gamma radiation treatment of the UHMWPE and is further affected by aging.

It is apparent from the tension fatigue data (Fig. 4(a)–(d)) that the inception for crack propagation occurs at significantly greater values of stress intensity range for Hylamer®-M for all sterilization conditions. This indicates that the enhanced crystallinity is beneficial for fatigue resistance. Further, the stable crack growth regime for Hylamer®-M is shifted to greater values of stress intensity range over the GUR4150HP. This indicates that for an identical crack length and loading condition, the rate of crack propagation will be substantially lower for Hylamer®-M. Further, it is evident that the gas plasma sterilization and ethylene oxide sterilization methods do not significantly reduce the fatigue resistance while gamma radiation results in a substantial degradation of the fatigue resistance of UHMWPE. One interesting finding of this study is that gamma sterilization in an inert environment provided no substantial improvement over the gamma radiation in air for both unaged Hylamer®-M and GUR4150HP. The detrimental effects of ionizing radiation in the unaged condition are most likely due to the embrittlement associated with initial oxidation

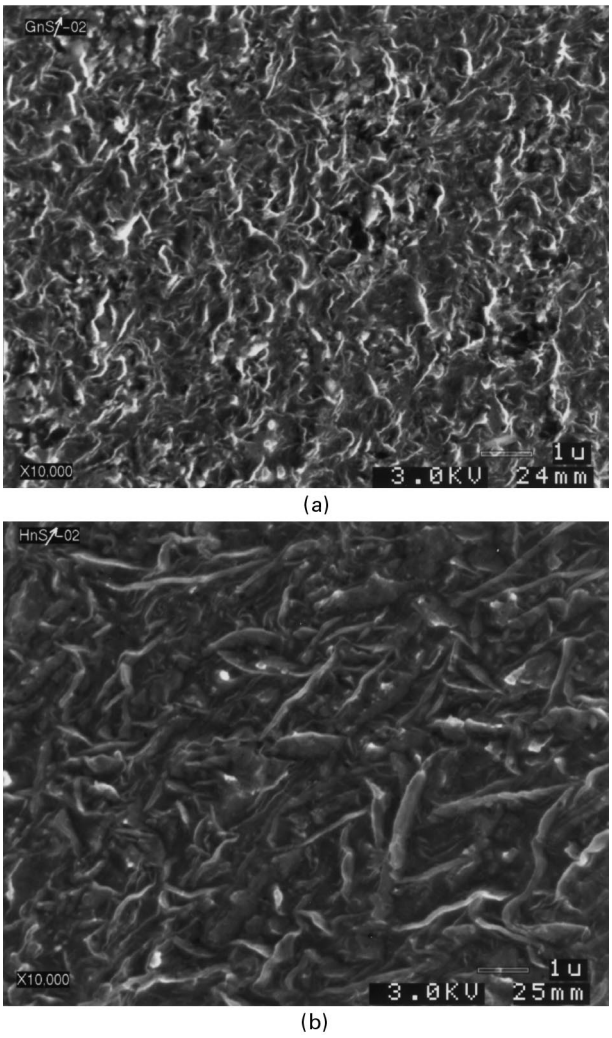

Fig. 11. Field emission micrographs showing the lamellae structure of: (a) GUR4150HP; and (b) Hylamer®-M. Note the larger crystalline structures in the Hylamer®-M.

and scission for the gamma-air condition, and the crosslinking associated with the gamma-inert condition.

The accelerated aging strongly affects the fatigue resistance of both polymers. Drastic embrittlement (and surface cracking) is found for all specimens gamma sterilized in air and subsequently aged. For both polymers, the effect of accelerated aging in combination with gamma sterilization in air results in severe degradation of the fatigue crack propagation resistance. Additionally, as previously mentioned, the fractured specimens reveal that the accelerated aging results in a clear transition of near-surface and interior fracture micromechanisms possibly linked to the profile of the sterilization induced free radicals and diffusion of oxygen in the accelerated aging process. Gamma sterilization in an inert environment followed by aging results in a decrease in fatigue resistance in comparison to the unaged condition but offers substantial improvement over the gamma-air aged condition (Table 2). Further, it is evident that EtO and gas plasma are highly resistant to degradation

Table 3
Density of GUR4150HP and Hylamer®-M for the unaged and aged conditions

Sterilization (aging)	Density g/cm^3	
	Interior section (A)	Exterior section (B)
GUR4150HP		
Non-sterile (unaged)	0.932	0.933
Non-sterile (aged)	0.924	0.933
Plasma (unaged)	0.932	0.932
Plasma (aged)	0.919	0.933
EtO (unaged)	0.933	0.935
EtO (aged)	0.926	0.932
Gamma-air (unaged)	0.934	0.936
Gamma-air (aged)	0.933	0.969
Gamma-inert (unaged)	0.938	0.938
Gamma-inert (aged)	0.935	0.936
Hylamer®-M		
Non-sterile (unaged)	0.930	0.936
Non-sterile (aged)	0.934	0.941
Plasma (unaged)	0.930	0.936
Plasma (aged)	0.930	0.935
Gamma-air (unaged)	0.939	0.938
Gamma-air (aged)	0.949	0.972
Gamma-inert (unaged)	0.940	0.942
Gamma-inert (aged)	0.950	0.945

brought about through accelerated aging. An interesting finding is that accelerated aging does result in a slight degradation of fatigue properties of the non-sterile groups and groups not subjected to ionizing radiation. This suggests that microstructural evolution is brought about through the accelerated aging process.

All the aged material groups exhibit two distinct regions of optical translucence as shown in Fig. 2. This transition in optical translucence is seen optically but not during SEM. However, micromechanistic transitions between the interior and near surface portions of the fracture plane are observed for the gamma sterilized specimens. Near the surface (region B in Fig. 2), the fracture surface of the gamma-air specimens appears cellular in nature with the remnants of many small fibrils orthogonal to the crack plane (Fig. 8(a) and (c)). The cellular structure increases in size as it approaches the less oxidized interior. The interior region exhibits the more familiar scallop markings often observed in retrieved knee components [28,29]. It is of interest to note that the scallops opened up in the direction of crack growth. Fig. 8(a) shows that in the Paris regime, the scallops open up nearly perpendicular to the direction of crack growth. This indicates that the crack effectively propagates from the outer, more brittle region, to the inner region and then along a left-to-right path. The Hylamer®-M gamma-air sterilized material exhibited similar behavior. These specimens have an outer ring of highly embrittled material as seen in Fig. 9(a). This results in the cellular appearance of the fracture surface (Fig. 9(b)) and a change in micromechanism from the surface to the interior (Fig. 9(a)). This gradient of cellular texture might be an indication that the crack

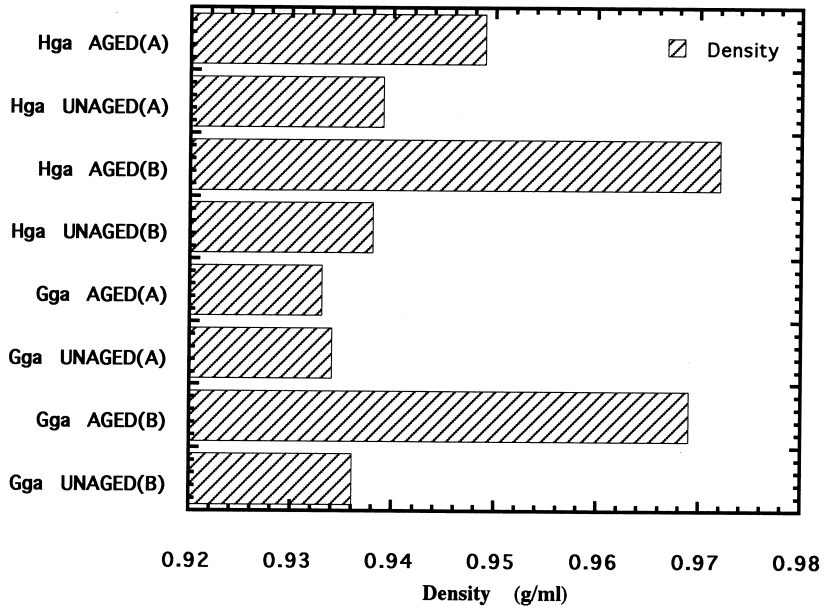

Fig. 12. Bar graph showing the effect of accelerated aging on polymer density of specimens sterilized by gamma radiation. Samples were measured in the interior (A) and exterior (B) portions of the specimen (Fig. 1).

advances inward to the interior before moving in the left-to-right direction. Extensive surface cracking is noted during fatigue testing of both gamma-air sterilized polymers supporting the fact that the crack grows along the brittle surface of the specimen, then into the interior. This phenomenon results in severe embrittlement and brittle fatigue behavior of both polymers (Fig. 4(b) and (d)).

In contrast to the large zone of embrittlement observed in the gamma-air sterilized condition, the zone in the inert gamma sterilized groups is a fraction of the size. This could be due to the fact that the inert environment allows for crosslinking to occur near the surface reducing the free radical population and diminishing the propensity for oxidation during the aging process. No cellular features and little to no gradient of micromechanisms are observed in the inert specimen subjected to accelerated aging (Fig. 10(a)). Optical micrographs show no evidence of surface cracking. The scallop markings are present in the interior region although they do not tend to open in any specific direction (Fig. 10(b)). For this material (Hylamer®-M gamma sterilized in an inert environment and aged) the specimens fracture abruptly and exhibit a drastic increase in the fatigue crack propagation slope (Table 2).

Fatigue degradation brought about by gamma radiation and accelerated aging is accompanied by structural evolution of the UHMWPE. Density gradient column measurements indicate that density increases as a result of gamma sterilization and that accelerated aging enhances this effect. FTIR demonstrates that oxidation levels increase substantially as a result of ionizing radiation and aging. Further accelerated aging results in a gradient of density and oxidation level through the specimen thickness. The increased oxidation in the aged specimens leads to embrittlement and deterioration of fatigue fracture resistance of UHMWPE.

Another important finding of this study is the effect of temperature on fatigue crack propagation. It is clearly shown that specimens tested at lower temperature (room temperature) will have greater resistance to inception of crack propagation. The reduction in crack growth resistance observed in the body temperature tests is believed to be associated with enhanced viscoelastic mechanisms. At the

Table 4
Oxidation indices of GUR4150HP and Hylamer®-M for the unaged and aged conditions. Standard deviation in parentheses

Material group	GUR4150HP		Hylamer®-M	
	CA/mil	Ketone abs/mil	CA/mil	Ketone abs/mil
Non-sterile unaged	0.180 (0.016)	0.027 (0.002)	0.098 (0.020)	0.017 (0.002)
Non-sterile aged	0.137 (0.012)	0.041 (0.009)	0.071 (0.009)	0.015 (0.002)
Gas plasma aged	0.210 (0.055)	0.045 (0.010)	0.178 (0.016)	0.028 (0.004)
EtO aged	0.156 (0.042)	0.015 (0.005)	–	–
Gamma-inert aged	0.818 (0.038)	0.300 (0.011)	0.758 (0.029)	0.274 (0.010)
Gamma-air aged	5.848 (0.979)	1.788 (0.043)	3.698 (0.979)	1.233 (0.059)

crack tip, the level of ductility and local creep mechanisms are enhanced by elevated temperature conditions and can assist in near-tip fracture processes. These enhanced mechanisms render the polymer less tolerant to crack propagation at body temperature in comparison to room temperature. This finding has important implications as the majority of published fatigue data on UHMWPE is for room temperature (air) environments. Fatigue predictions based on room temperature data could result in an overestimation of the implant life.

Such degradation of fatigue fracture resistance of the orthopedic polymers when subjected to sterilization, subsequent aging and body temperature environments increases the likelihood of cyclic damage in vivo. This is of critical concern for UHMWPE inserts used in total knee replacements where complex cyclic stresses are known to exist and where fatigue mechanisms can result in delamination and the generation of debris, which can severely limit the longevity of the implant.

5. Conclusions

It is clear from this work that morphology, sterilization, aging and test all play a critical role in the fatigue resistance of medical grade UHMWPE. Higher crystallinity appears to aid in the resistance to fatigue crack propagation resistance. Hylamer®-M offers increased resistance to fatigue fracture due to its enhanced lamellae thickness associated with heightened crystallinity and yield strength. Sterilization also plays an important role in fatigue in that ionizing radiation alters the structure through oxidation, scission and crosslinking, and further results in a polymer structure with decreased tolerance to cyclic damage. Accelerated aging intensifies this process and drastically affects the fatigue performance of specimens sterilized by gamma radiation in air. Further, testing at body temperature enhances near-tip fracture processes and degrades the fatigue resistance of UHMWPE. This finding indicates that orthopedic polymers should be evaluated under in vivo conditions whenever possible in order to make accurate life predictions. In summary, the results presented indicate that choice of polymer morphology and choice of sterilization technique play a crucial role in the fatigue performance and long term structural integrity of orthopedic implants.

Acknowledgements

The authors would like to thank Ms Dezba Coughlin for her assistance with the fatigue testing. The assistance of Ms Kerry Hughes and Ms Nazanine Matin in the fatigue studies is also greatly appreciated. This work was supported by Depuy Orthopaedics, Inc. and the National Science Foundation grant #CMS-9624978 to the University of California.

References

[1] Bartell DL, Bicknell VL, Wright TM. J Bone Jnt Surg 1986;68:1041.
[2] Pruitt L, Koo J, Rimnac CM, Suresh S, Wright TM. J Orth Res 1995;13:143.
[3] Pruitt L, Suresh S. Phil Mag 1993;67:1219.
[4] Pruitt L, Hermann R, Suresh S. J Mater Sci 1992;27:1608.
[5] Bartell DL, Rimnac CM, Wright TM. In: Goldberg VM, editor. Controversies of total knee arthroplasty, New York: Raven Press, 1991. p. 61.
[6] Sauer JA, Hara M. Adv Polym Sci 1990;91/92:71.
[7] Pruitt L, Bailey L. Polymer 1998;39:1545.
[8] Ries M, Weaver K, Rose RM, Gunther J, Sauer W, Beals N. Clinical Orthoped Rel Res 1996;333:87.
[9] Goldman M, Pruitt L. J Biomed Mater Res 1998;40(3):378.
[10] Dole M, editor. Radiation chemistry of macromolecules. New York: Academic Press, 1972.
[11] Shinde A, Salovey RJ. J Polym Sci 1985;23:1681.
[12] Birkinshaw C, Buggy M, Daly S, O'Neill M. Polymer Degrad Stabil 1988;22:285.
[13] McKellop HA, Shen FW, Salovey R. Transactions of the 44th Annual Meeting of the Orthopedic Research Society, New Orleans, 1998, p. 98.
[14] Jasty M, Bragdon CR, O'Connor DO, Muratoglu OK, Premnath V, Merrill E, Harris WH. Transactions of the 43rd Annual Meeting of the Orthopedic Research Society, San Francisco, 1997, p. 785.
[15] Wang A, Polineni VK, Essner A, Sun DC, Stark C, Dumbleton JH. Transactions of the 23rd Annual Meeting of the Society for Biomaterials, San Francisco, 1997.
[16] Ediden AA, Pruitt L, Jewett CW, Crane DJ, Roberts D, Kurtz SM. J Arthroplasty 1999;14:4.
[17] Dawes K, Glover LC. In: Mark JE, editor. Physical properties of polymers handbook. New York: AIP Press, 1966. p. 557.
[18] Baker D, Coughlin D, Pruitt L. Transactions of the 24th Annual Meeting of the Society for Biomaterials, San Diego, 1998, p. 122.
[19] Dunlap PH, Rimnac C. Transactions of the 44th Annual Meeting of the Orthopedic Research Society, New Orleans, 1998, p. 787.
[20] Schmalzried TP, Jasty M, Rosenberg A, Harris WH. J Appl Biomater 1994;5:185.
[21] Sun DC, Schmidig G, Stark C, Dumbleton JH. Transactions of the 42nd Annual Meeting of the Orthopedic Research Society, Atlanta, 1996, p. 119.
[22] Sanford WM, Saum KA. Transactions of the 41st Annual Meeting of the Orthopedic Research Society, 1995, p. 119.
[23] Furman BD, Lelas J, McNulty D, Smith T, Li S. Transactions of the 44th Annual Meeting of the Orthopedic Research Society, New Orleans, 1998, p. 102.
[24] Kurtz SM, Bartel DL, Rimnac CM. Transactions of the 40th Annual Meeting of the Orthopedic Research Society, San Francisco, 1994, p. 584.
[25] Audouin L, Langlos V, Verdu J, de Broun JCM. J Mater Sci 1994;29:569.
[26] Connelly GM, Rimnac CM, Wright TM, Hertzberg RW, Manson JA. J Orth Res 1984;2:119.
[27] Zeng ZP, Buggy M, Griffin J, Little EG. J Mater Sci: Mater Med 1992;3:255.
[28] Rimnac CM, Wright TM, Klein RW. Polym Engng Sci 1988;28:1586.
[29] Wright TM, Rimnac CM, Stulberg SD, Mintz L, Tsao AK, Klein RW, McCrae C. Clin Orthopedics 1992;276:126.